Electromagnetic Analysis of the Superconducting Magnet Feeders System of the Divertor Tokamak Testing Facility

G. De Marzi[1], A. Cucchiaro[2,3], F. De Baggis[4], A. della Corte[1], L. Giannini[1], L. Muzzi[1], and A. Di Zenobio[1]
1. Department of Fusion and Technology for Nuclear Safety and Security, ENEA, Frascati, RM, Italy
2. DTT S. C. a r. l., Frascati, RM, Italy
3. Consorzio CREATE, Naples, Italy
4. Department of Mechanical Engineering, Sapienza Università di Roma, RM, Italy

Introduction

In controlled nuclear fusion reactors based on magnetic confinement, the hot, dense and stable plasma of hydrogen isotopes is confined by strong magnetic fields in a torus-shaped vacuum vessel. Among the various magnetically confined configurations, such devices (called *Tokamaks*) are able to provide the best performances.

As part of the European Research Roadmap to the Realization of Fusion Energy [1], the Divertor Tokamak Test facility (DTT) [2] aims to study alternative divertor configurations in view of the EU-DEMO [3] power exhaust handling issues.

In a Tokamak, the magnetic field is generated by a system of coils which can be divided into three main groups:

- the Toroidal Field (TF) coils, producing a stationary and uniform field. The magnitude of the stationary toroidal field is typically of the order of 10 Tesla;
- the Central Solenoid (CS), placed along the axis of the torus, acting as the primary of a transformer, where the plasma is the secondary;
- the Poloidal Field (PF) coils installed around the torus, which provide control of the plasma shape and position.

As shown in Figs. 1-2, the DTT superconducting magnet system comprises 18 TF coils, 6 PF coils (PF1-6), and six CS modules (from top to bottom: CS3U, CS2U, CS1U, CS1L, CS2L, CS3L).

The superconducting coils are connected to the current leads by a system of superconducting current feeders, which are currently being designed (figure 1). To finalize the project in the most appropriate way, it is advisable to carry out a detailed evaluation of the magnetic field seen by the feeders along their paths. This information is of great relevance for:

- the choice of the best superconducting material to use;
- the definition of the best paths for the current feeders;
- the design of the mechanical supports that counteract the Lorentz loads when the coils are energized at operation.

The paths of the feeders are shown in Fig. 2, together with the Toroidal Field Coil, the Poloidal Field Coils, and the Central Solenoid modules. The feeders' main parameters are resumed in Tables 1-3 (the reported lengths refer to the paths inside the cryostat and do not take into account the path from the cryostat to the Current Leads).

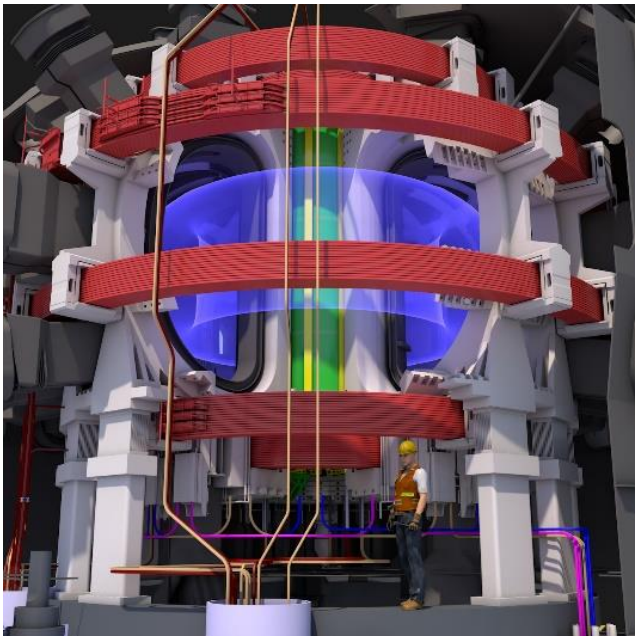

Figure 1. The DTT superconducting magnet system comprises 18 Toroidal Field (TF) coils, 6 Poloidal Field (PF) coils, and a Central Solenoid (CS). *Source: DTT Plant Integration Document ver. 2.4*.

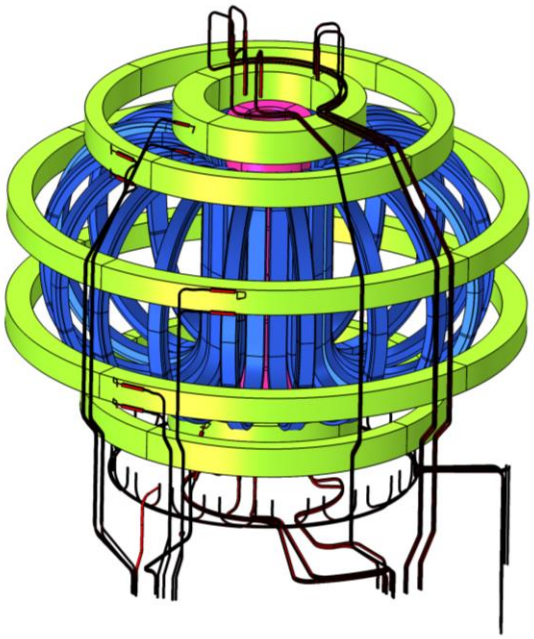

Figure 2. The DTT magnet system and its current feeders, as modelled in Comsol using the geometric entities of the software: TF coils (blue); PF coils (green); CS (magenta); and feeders (black).

Numerical Model

In this work, the magnetic field interface (*mf*) of the AC/DC module of COMSOL Multiphysics® has been used to calculate the magnetic field profiles along the paths of the current feeders, in some particular time instants of the most important plasma scenarios.

The physics interface solves Maxwell's equations, which are formulated using the magnetic vector potential $\boldsymbol{A}$

$$\nabla \times \left(\frac{1}{\mu}\nabla \times \boldsymbol{A}\right) = \boldsymbol{J} \qquad (1)$$

and the constitutive relation

$$\boldsymbol{B} = \mu \boldsymbol{H}, \qquad (2)$$

where $\boldsymbol{B}$ is the magnetic flux density, $\boldsymbol{H}$ is the magnetic field, $\boldsymbol{J}$ is the external current density, and μ is the magnetic permeability.

Given the complexity of a full 3D model, we have considered the total field as the superposition of a toroidal component and a poloidal component.

The toroidal field has been calculated by means of a 3D model, by taking advantage of the 18-fold symmetry of the TF coil system. The *Perfect Magnetic Conductor* boundary condition has been exploited, whereas a homogenized multi-turn model with a "numeric" coil type has been used to excite the coil with 42.5 kA.

In a two-step study, a coil geometry analysis has been carried out before the stationary study.

Table 1: Main parameters of the CS feeder pairs

Coil ID#	Length [m] (*in*)	Length [m] (*out*)	Feeder pairs
CS3U	17.3	16.9	6×2
CS2U	14.2	13.9	6×2
CS1U	14.4	14.0	6×2
CS1L	10.2	9.9	6×2
CS2L	6.8	6.5	6×2
CS3L	6.6	7.0	6×2

Table 2: Main parameters of the PF feeder pairs

Coil ID#	Length [m] (*in*)	Length [m] (*out*)	Feeder pairs
PF1	10.3	10.0	6×2
PF2	9.0	9.5	6×2
PF3	6.6	7.1	6×2
PF4	4.5	4.9	6×2
PF5	2.3	*N. D.*	6×2
PF6	3.8	4.3	6×2

Table 3: Main parameters of the TF feeder pairs and jumpers

Coil ID#	Length [m] (in)	Length [m] (out)	Feeder pairs
Group 1	6.0	4.3	3×2
Group 2	6.1	6.0	3×2
Group 3	5.3	6.8	3×2
Jumpers	~3		3×5

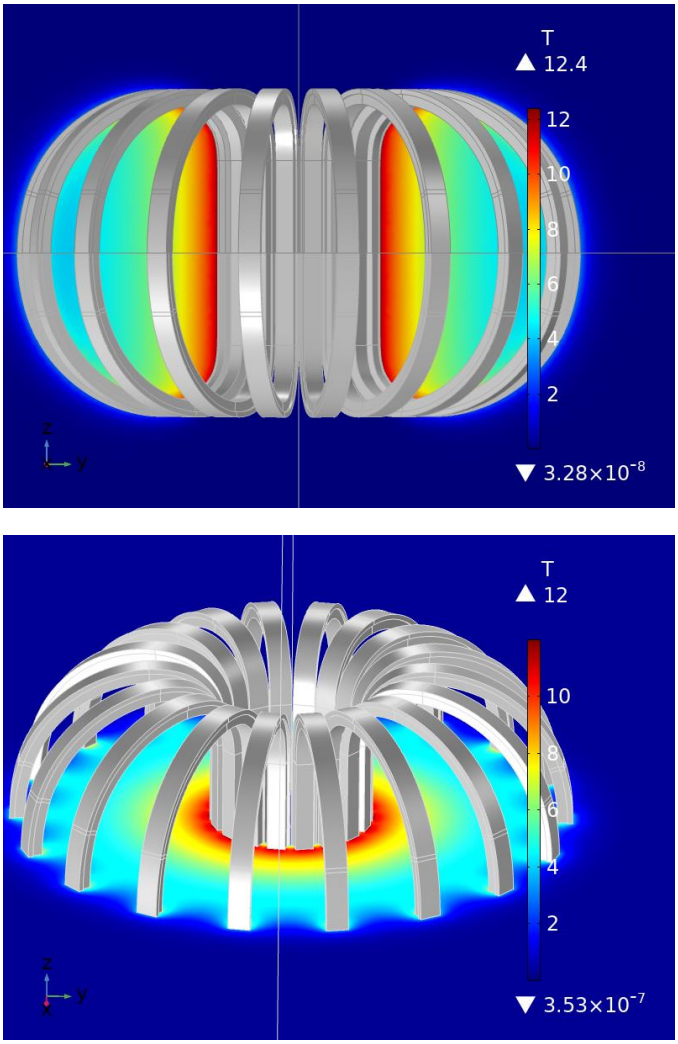

Figure 3. The magnetic field generated by the 18 TF coils, when the coils are energized with a steady 42.5 kA current. The high-field region is inside the coils, and the field outside drops to very low values. The finite number of the TF coils cause a periodic variation of the toroidal field from its nominal value called toroidal field ripple.

The poloidal field contribution generated by the PF and CS coils has been evaluated by using a 2D-axisymmetric component, exploiting the *mf* interface of AC/DC module with the homogenized multi-turn coils feature. In the stationary study, the different time instants of the main normal operation scenarios have been taken into account in a parametric sweep.

The paths of the feeders have been drawn in a 3D component, and a General Extrusion operator (*genext1*) has been employed to map the magnetic field from the 2D axisymmetric domain to the 3D domain, for the calculation of the field along the feeders' paths. This procedure allows for achieving considerable computational savings.

Simulation Results

The cases analyzed are those of the normal operation scenarios (Single Null, Double Null, Snow Flake, X-Divertor, Negative Triangularity), at the time instants defined by the Scenario v9 (year 2019) [4]. In the following sub-sections, the toroidal and poloidal field contributions will be considered separately, by means of two different Finite Elements Models (FEM) (18-fold 3D and 2D-axisymmetric FEMs,

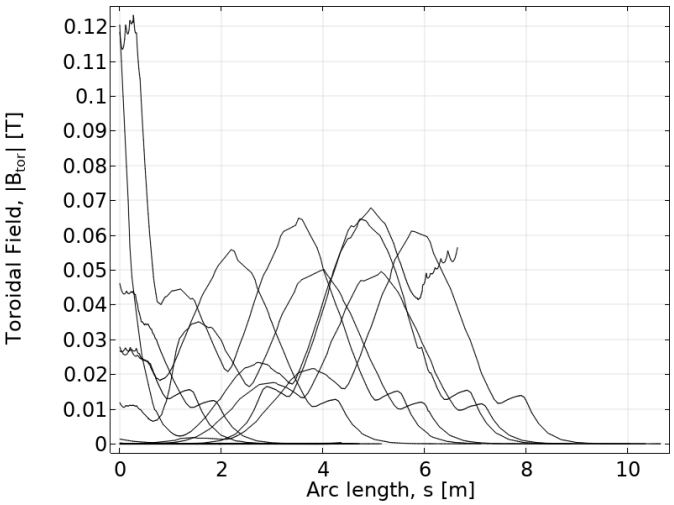

Figure 4. The $|B_{tor}|$ curves evaluated along the PF, CS, and TF feeders' arclengths.

respectively). Moreover, since the operating scenarios should be guaranteed with a 10% margin due to feedback control specifications, the current values of the PF coils have been increased by 10%.may include color simulation images.

Toroidal Field Coils contribution

The spatial arrangement of the feeders' paths breaks the 18-fold symmetry of the magnetic field; therefore, in principle it would be necessary to implement a full 3D FEM model. To save computational time, a reasonable approach is to separate the TF coils contribution from the PF and CS coils one and verify, in the areas interested by the feeders, that the former can be safely neglected. Hence, the toroidal field generated by the TF coils at full current (about 42.5 kA) was assessed using an 18-fold 3D model. The magnetic field map thus obtained is shown in Figure 3, whereas the norm of the toroidal field, $|B_{tor}|$ evaluated along the feeders' arc lengths, is reported in Figure 4. The arc length is here defined as the length of a feeder: $s = \int_{\gamma} \overrightarrow{dl}$, where $\overrightarrow{dl}$ is a differential displacement vector along a curve γ ($s = 0$ at the coil terminal joint). As it can be clearly seen in Figure 4, $|B_{tor}|$ always stays below 70 mT, except for the PF1 and PF2 feeders, for which $|B_{tor}|$ reaches a peak of approximately 120 mT (close to the coils). In light of the results obtained, the contribution of $|B_{tor}|$ will be neglected in the rest of the discussion.

Poloidal Field Coils contribution

Unlike the TF magnets, where currents are stationary, in all PF and CS coils the current varies over time, so that the poloidal field contribution, $|B_{pol}|$ is a function of time. It is also necessary to take into account the contribution of the plasma current, which must be added to $|B_{pol}|$. The currents circulating in the coils in the various scenarios and at different selected time instants are listed in Tables 4-6.

Figures 5-8 shows the magnitude of the poloidal magnetic field $|B_{pol}|$ along the path of the feeders, for all scenarios at any time. The highest fields are obtained in the Double Null scenario at t = 27 s (CS feeders), and in the Single Null scenario at the end of flat top (PF and TF feeders).

Regarding the CSL, PF and TF feeders, the highest values for $|B_{pol}|$ are found to be close to the coil terminal joints, with peaks of 4.3 T (CSL), 2.9 T (PF), and 1.25 T (TF feeders and jumpers). On the CSU feeders, the peak reaches 5.6 T, in the regions where the feeders are very close to the PF1 coil (see Figure 9).

Table 4: Rated currents for the Single Null scenario, at different time instants (t = 0 s: premagnetization; t = 15 s: X-point formation, XPF; t = 28 s: start of heating, SOH; t = 36 s: start of flat-top, SOF; t = 78.5 s: end of flat-top, EOF).

Time [s]	0	15	22	27	28	37	78.5
I_{pl} [MA]		3.00	4.30	5.50	5.50	5.50	5.50
CS3U [kA]	29.04	13.58	11.40	0.19	0.44	24.81	6.50
CS2U [kA]	29.04	6.55	7.09	5.61	5.06	-9.12	-24.41
CS1U [kA]	29.04	5.24	-2.99	-14.62	-15.38	-17.55	-29.04
CS1L [kA]	29.04	2.21	-13.32	-22.26	-22.79	-21.09	-29.04
CS2L [kA]	29.04	7.51	5.47	-8.24	-9.04	-14.54	-29.04
CS3L [kA]	29.04	21.31	10.06	15.89	15.29	9.80	-6.19
PF1 [kA]	4.61	15.50	12.34	16.02	15.51	15.04	19.73
PF2 [kA]	6.03	-5.88	-9.71	-13.11	-13.16	-18.51	-24.21
PF3 [kA]	0.00	-4.67	-6.12	-9.84	-9.85	-7.98	-6.97
PF4 [kA]	0.00	-5.26	-6.84	-7.10	-7.03	-10.91	-11.53
PF5 [kA]	6.03	-10.98	-17.35	-23.63	-23.93	-21.76	-24.01
PF6 [kA]	4.61	18.07	24.28	28.30	28.30	28.30	28.30

Table 5: Rated currents for the Double Null scenario, at different time instants (t = 0 s: premagnetization; t = 15 s: X-point formation, XPF; t = 28 s: start of heating, SOH; t = 36 s: start of flat-top, SOF; t = 93.7 s: end of flat-top, EOF).

Time [s]	0	15	22	27	28	37	78.5
I_{pl} [MA]		3.00	4.30	5.00	5.00	5.00	5.00
CS3U [kA]	29.04	16.01	18.32	19.06	18.50	15.36	-6.03
CS2U [kA]	29.04	5.06	-3.72	-9.61	-10.49	-15.76	-29.04
CS1U [kA]	29.04	4.13	-6.06	-11.53	-12.11	-13.16	-28.59
CS1L [kA]	29.04	4.13	-6.06	-11.53	-12.11	-13.16	-28.59
CS2L [kA]	29.04	5.06	-3.72	-9.61	-10.49	-15.76	-29.04
CS3L [kA]	29.04	16.01	18.32	19.06	18.50	15.36	-6.03
PF1 [kA]	4.61	22.55	26.07	28.30	28.30	28.30	25.09
PF2 [kA]	6.03	-14.26	-21.13	-24.29	-24.61	-24.37	-25.20
PF3 [kA]	0.00	-3.63	-4.86	-5.95	-5.89	-7.16	-7.69
PF4 [kA]	0.00	-3.63	-4.86	-5.95	-5.89	-7.16	-7.69
PF5 [kA]	6.03	-14.26	-21.13	-24.29	-24.61	-24.37	-25.20
PF6 [kA]	4.61	22.55	26.07	28.30	28.30	28.30	25.09

Table 6: Rated currents for the Snow Flake, X-Divertor, and Negative Triangularity scenarios, at start of flat top (SOF) and end of flat top (EOF).

Time [s]	Snow Flake		X-Divertor		Neg. Triangularity	
	SOF	EOF	SOF	EOF	SOF	EOF
I_{pl} [MA]	4.50	4.50	4.50	4.50	5.00	5.00
CS3U [kA]	-18.04	29.04	-20.37	29.04	13.07	-19.56
CS2U [kA]	28.94	-4.89	24.95	-4.37	-7.13	-19.44
CS1U [kA]	-18.80	-29.04	-16.55	-28.98	0.92	-15.57
CS1L [kA]	-29.04	-29.04	-29.04	-29.04	-12.14	-29.04
CS2L [kA]	17.46	-7.81	15.71	-6.77	-23.39	-29.04
CS3L [kA]	29.04	29.04	29.04	29.04	-20.00	-29.04
PF1 [kA]	0.94	-15.32	0.99	-22.35	-5.13	2.72
PF2 [kA]	-10.61	-4.98	-9.99	3.34	10.19	-0.40
PF3 [kA]	2.21	0.59	2.62	-1.67	-12.17	-8.77
PF4 [kA]	-28.12	-28.60	-28.36	-28.60	-21.63	-25.08
PF5 [kA]	27.10	25.55	25.33	25.73	23.00	27.10
PF6 [kA]	-11.27	-14.19	-9.96	-14.33	16.27	4.64

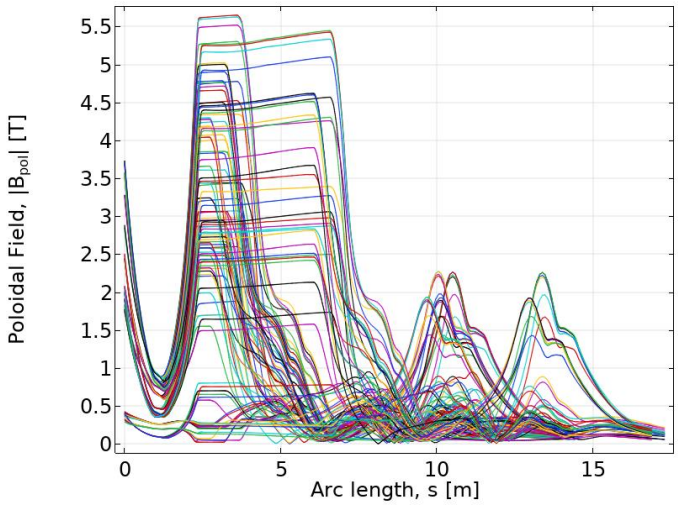

Figure 5. $|B_{pol}|$ calculated for all scenarios at any time, along the entire arc lengths of the CSU feeders.

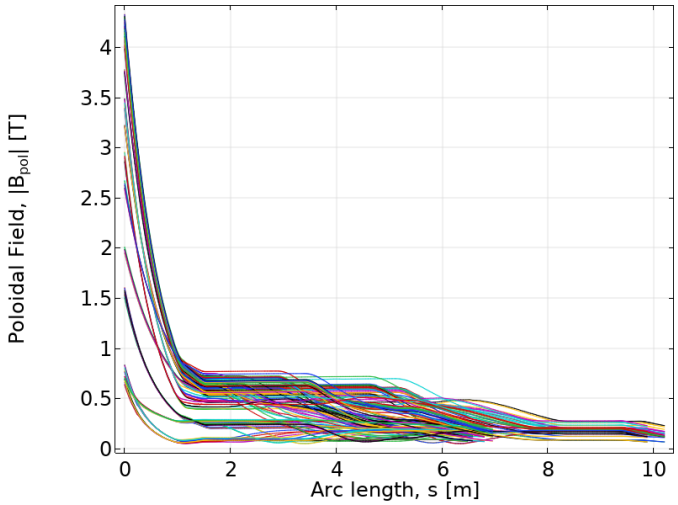

Figure 6. $|B_{pol}|$ calculated for all scenarios at any time, along the entire arc lengths of the CSL feeders.

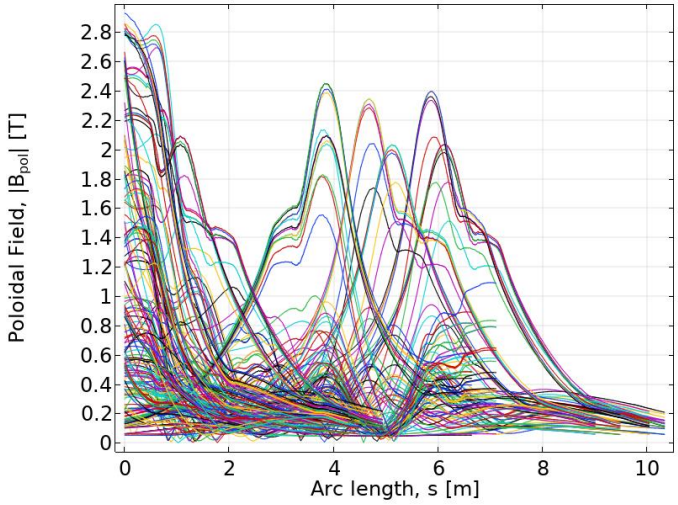

Figure 7. $|B_{pol}|$ calculated for all scenarios at any time, along the entire arc lengths of the PF feeders.

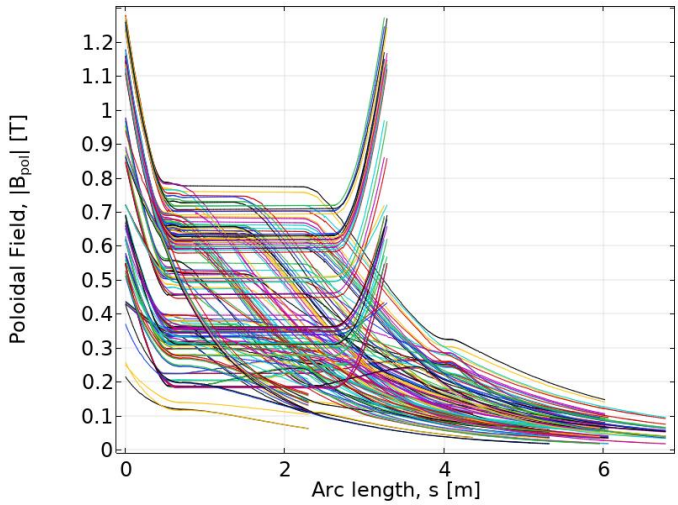

Figure 8. $|B_{pol}|$ calculated for all scenarios at any time, along the entire arc lengths of the TF feeders and jumpers.

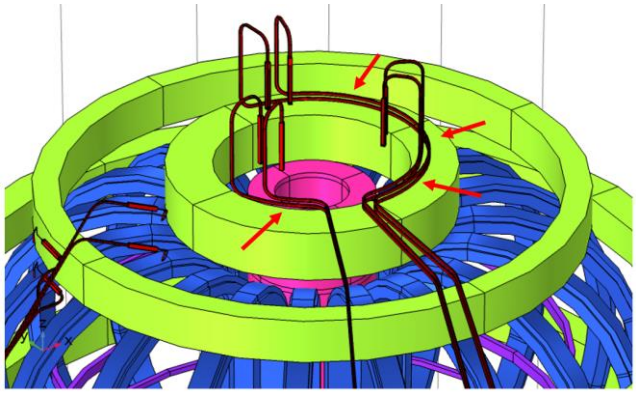

Figure 9. Before reaching the CSU coil termination joints, the feeders pass just above PF1 (red arrows in the picture), where the magnetic field can reach values as high as 5.5 T (Double-Null scenario at t = 27 s). The paths close to PF1 correspond to the *plateaux* of the *field vs. arc length* curves of Figure 5.

Conclusions

For the conceptual design of the current feeders of the DTT magnet system, we evaluated the field seen by the current feeders along their paths from the cryostats to the coil termination joints. In order to simplify the simulations, the total magnetic field has been calculated by separating the contributions of the toroidal and poloidal field coils ($|B_{tor}|$ and $|B_{pol}|$) have been evaluated separately. It is found that the contribution of $|B_{tor}|$ can be safely neglected, as it always stays below 70 mT, except for the PF1 and PF2 feeders (for which $|B_{tor}|$ reaches a peak of approximately 120 mT).
The magnitude of $|B_{pol}|$ along the path of the feeders has been calculated for all scenarios at any time. The PF currents have been increased by 10% to guarantee enough margin for the feedback control systems. The highest values for $|B_{pol}|$ have been obtained in the Double Null scenario at t = 27 s (CS feeders), and in the Single Null scenario at EOF (PF and TF feeders). Regarding the CSL, PF and TF feeders, the highest values for $|B_{pol}|$ are found to be close to the coil terminal joints,

with peaks of 4.3 T (CSL), 2.9 T (PF), and 1.25 T (TF feeders and jumpers). On the CSU feeders, the peak reaches 5.6 T, in the regions where the feeders are very close to the PF1 coil. Since only a small portion of the feeders' arc lengths are subject to large $|B_{pol}|$, each feeder could be split into two sections joined by a properly designed joint. Different superconducting materials could be used for the different sections (*i.e.*, NbTi for the low-field section, and Nb_3Sn or HTS tapes for the high-field section closest to the magnets). As a final consideration, it is worth noting that the contribution of the field generated by the feeders themselves (*self-field*, B_{sf}) was not considered. This analysis will be the subject of a dedicated FEM study. However, from the analytic expression for the magnetic field generated by a current carrying cable, the expected self-field is of the order of 100 mT for a current of 30 kA ($B_{sf} \sim \mu_0 i/(2\pi r)$).

Acknowledgements

This work is carried out in the frame of the DTT activity. The authors are very grateful to all the colleagues is involved in the DTT project for their precious contribution.

References

1. https://www.euro fusion.org/eurofusion/roadmap/
2. R. Albanese *et al*., *Design review for the Italian Divertor Tokamak Test facility*, Fus. Eng. Des. **146 A**, 194, (2019).
3. G. Federici *et al*., *DEMO design activity in Europe: Progress and updates*, Fus. Eng. Des., **136 A**, 729, (2018).
4. R. Martone, R. Albanese, F. Crisanti, A. Pizzuto, and the DTT team, *Divertor Tokamak Test facility Interim Design Report*, ISBN: 978-88-8286-378-4, Publisher: ENEA Frascati Research Center, 2019. Available online at: *https://www.dtt-project.enea.it/downloads/DTT_IDR_2019_WEB.pdf*